2011 American Control Conference
on O'Farrell Street, San Francisco, CA, USA
June 29 - July 01, 2011

Optimal control for batch crystallization with size-dependent growth kinetics

Naim Bajcinca and Steffen Hofman

***Abstract*— An efficient algorithm for the optimal control of a batch crystallization process with size-dependent growth kinetics is proposed. By means of a unique diffeomorphism, new independent coordinates for the time and size variables of the underlying population balance equation are introduced, leading to a closed infinite dimensional moment model. The posed optimal control problem is solved using the minimum principle for a simplified model with neglected natural feedback of the nucleation mass into the crystallization kinetics. The solution is obtained in analytical form, and it is shown to be unique. Additionally, for the original optimization problem involving the full process dynamics, a simple feasible sub-optimal solution, as well as a lower and an upper bound for the cost, are suggested.**

I. Introduction

A. Population balance equation

A batch crystallizer is made up of a large number of crystal particles immersed in a dispersed phase system, constituted by a continuous solvent liquid medium (typically, water) and dispersed solute crystalline entities (molecules or ions), in which, with regard to the crystal growth and nucleation phenomena, a mass transfer of the solute from the liquid to a pure solid crystalline phase occurs, see *e.g.* [1]. Such a crystallization process is commonly modeled by a *population balance equation* (PBE) of the form (see *e.g.* [2])

$$\frac{\partial f}{\partial t}+\frac{\partial\left(Gf\right)}{\partial \ell}=0,\ \ell>0,\ t>0, \tag{1a}$$

with the associated boundary and initial conditions

$$f(t,0)=\frac{B(t)}{G(t,0)},\ t\geq 0, \tag{1b}$$

$$f(0,\ell)=f_0(\ell),\ \ell\geq 0, \tag{1c}$$

where each particle is assigned the *size* (or, the internal) coordinate ℓ. The function $f=f(t,\ell)$ represents the *population density function* or *particle size distribution*, defined as the number density of particles per unit length ℓ. The term $f_0(\ell)$ stands for the given *initial density function* of the crystal seeds. The birth rate term $B=B(t)$ counts the number of born particles at the size $\ell=0$ in a unit time, and, hence, it impacts the boundary condition (1b). $G=G(t,\ell)$ in the advection term in (1a) represents the growth rate of the particle size which in general is a time- and size-dependent function. In this article, the following separability condition for $G(t,\ell)$ is assumed

$$G(t,\ell)=\gamma(\ell)G_0(t), \tag{2}$$

where $\gamma(\ell)>0$ and $G_0(t)>0$ stand for the *size-dependent* and *size-independent* factors, respectively. Note that, in practice, $\gamma(\ell)$ is given, while $G_0(t)$ is *a priori* not known. Without loss of generality, we assume $\gamma(0)=1$. The separability condition (2) is widely used in literature. For instance, this condition is satisfied by the Abegg-Stevens-Larson (abbr. ASL) model with $\gamma(\ell)=(1+\alpha\ell)^z, z<1$, the linear Canning-Randolph (abbr. C-R) model with $\gamma(\ell)=1+\alpha\ell$, *etc.*, see [1]. The latter linear model is well suited for validation purposes of the proposed integration and optimization algorithms in the article, since, therefore, closed solutions are obtainable.

An accurate prediction of the evolution of the population density function $f=f(t,\ell)$ for given initial and operating conditions in (1a-1c) can, in general, be challenging in that the distribution may extend over orders of magnitude in both, size and time, and changes in the distribution can be very sharp, see [3]. Different solution methods, such as the methods of moments and characteristics, and a variety of numerical discretization schemes (*e.g.* the finite volume schemes) have been developed in the past several decades (*e.g.* [3]).

Our work focuses on the method of characteristics and the method of moments, since some structural properties revealed thereby will be useful for the development of the essentially analytical integration and optimization schemes that we propose in this article. The method of characteristics is used to convert the PDE (1a) into a family of ODEs along the *characteristic curves* in the (t,ℓ)-plane. The method of moments, at the other hand, introduces a closed system of ODEs, involving the *moments* of the underlying density function $f{=}f(t,\ell)$, defined by the integral transforms

$$\mu_i(t)=\int_0^\infty \ell^i f(t,\ell)\mathrm{d}\ell,\quad i=0,1,2,\ldots. \tag{3}$$

Note that in a more complex setting, in particular, in the case of size-dependent growth rate which is considered here, the method of moments may get afflicted with the violation of the closure condition.

B. Process kinetics

The fundamental force for crystallization from the solution arises effectively from the level of supersaturation S, which

N. Bajcinca is with Max-Planck Institute for Dynamics of Complex Technical Systems, Sandtorstr.1, 39106 Magdeburg, Germany. (E-mail: *bajcinca@mpi-magdeburg.mpg.de*). S. Hofmann is with Technische Universität Berlin, Einsteinufer 17, 10857 Berlin, Germany. (E-mail: *hofmann@control.tu-berlin.de*). We gratefully acknowledge funding by the German Research Foundation under research grant DFG RA 516/7-1.

is a measure of the difference between the solution concentration (or mass fraction) c and saturation concentration ($c_{\rm sat}$), $S = c/c_{\rm sat}$ with $c = m_{\rm c}/(m_{\rm w}+m_{\rm c})$, where $m_{\rm w}$ is the solvent and $m_{\rm c}$ the solute mass. The saturation concentration $c_{\rm sat}$ can be controlled by the temperature T using the empirical model $c_{\rm sat}(T) = a_0 + a_1 T + a_2 T^2$, where a_0, a_1, and a_2 are given empirical parameters. Within the so-called metastable region of a moderately supersaturated solution, the nucleation rate B and the growth rate G_0 are driven by the supersaturation level according to

$$B(t)=k_b\,(S(t)-1)^b \mu_3(t),\;\; G_0(t)=k_g\,(S(t)-1)^g \qquad (4)$$

where k_g, g, k_b and b are positive empirical parameters, and μ_3 is the net 3rd moment of the density function. Note that for most substances $b > g$.

For the completion of the process model, the PBE (1a-1c) needs to be augmented by an additional algebraic equation for the mass balance, which implicitly impacts the *boundary term* B/G in (1b), and G in (1a), by providing a feedback from the solid to the liquid phase

$$m_{\rm c}(t) = m_0 - \rho k_v(\mu_3(t) - \mu_{3,0}) \qquad (5)$$

where $m_{\rm c}(t)$ is the mass dispersed in the continuous phase, $\mu_{3,0} = \mu_{3,{\rm s}}(0)$ is the initial 3rd moment of the crystal seeds, ρ is the particle mass density, and k_v is a volume shape factor, see [2].

C. Problem formulation

The population density function can be decomposed as $f(t,\ell) = f_{\rm n}(t,\ell) + f_{\rm s}(t,\ell)$, where $f_{\rm n} = f_{\rm n}(t,\ell)$ arises from the nucleation crystal particles, and $f_{\rm s} = f_{\rm s}(t,\ell)$ refers to the seed population. It is important to note that for the PBE (1a)-(1c), involving a source and an advection term only [no breakage and agglomeration!], the functions $f_{\rm n}$ and $f_{\rm s}$ do not "mix", in that no (t,ℓ) exists, where both $f_{\rm n}$ and $f_{\rm s}$ are non-zero. For the computation of $f_{\rm n}$ and $f_{\rm s}$, each can be associated a PBE, with a homogenous PDE of the form (1a), with the respective boundary/initial conditions: $f_{\rm n}(t,0) = B(t)/G(t,0)$, $t \geq 0$ and $f_{\rm n}(0,\ell) = 0$ for $f_{\rm n}$, and $f_{\rm s}(t,0) = 0$ and $f_{\rm s}(0,\ell) = f_0(\ell)$, $\ell \geq 0$ for $f_{\rm s}$. Since (1a) is linear, $f = f_{\rm n} + f_{\rm s}$ is a solution of the PBE (1a)-(1c).

As a consequence, using (3), the 3rd moment can be accordingly decomposed into $\mu_3 = \mu_{3,{\rm s}} + \mu_{3,{\rm n}}$, where

$$\mu_{3,{\rm n}}(t)=\int_0^\infty \ell^3 f_{\rm n}(t,\ell){\rm d}\ell,\;\; \mu_{3,{\rm s}}(t)=\int_0^\infty \ell^3 f_{\rm s}(t,\ell){\rm d}\ell. \qquad (6)$$

The general goal in a typical batch process is to produce a sufficiently large amount of "mass" $\mu_{3f} = \mu_3(t_f)$ within a reasonable time scope $0 \leq t \leq t_f$, while guaranteeing a certain level of product quality expressed, for instance, in terms of the *impurity* defined by ${\rm imp}_f = \mu_{3f,{\rm n}}/\mu_{3f,{\rm s}}$ where $\mu_{3f,{\rm n}} = \mu_{3,{\rm n}}(t_f)$ and $\mu_{3f,{\rm s}} = \mu_{3,{\rm s}}(t_f)$. Several [basically, equivalent] optimization scenarios based on such requirements arise, with two constraints and one cost function stated in terms of the variables t_f, $\mu_{3f,s}$ and $\mu_{3f,n}$.

In this paper, we consider the optimization problem

$$\underset{u(t)\in U,\, t\in[0,t_f]}{\text{minimize}}\; \mu_{3,{\rm n}}(t_f) \;\text{ subject to }\; \begin{matrix}\mu_{3,{\rm s}}(t_f)=\mu_{3f,{\rm sc}}\\ t_f = t_{f,c}\end{matrix} \qquad (7)$$

with fixed constants $\mu_{3f,{\rm sc}}$ and $t_{f,c}$, and the compact set U of admissible input values $u(t)$, $t \in [0,t_f]$. Obviously, in this scenario the final impurity ${\rm imp}_f = \mu_{3,{\rm n}}(t_f)/\mu_{3,{\rm s}}(t_f)$ could be equivalently used as penalization. Note further, that in our scenario we explicitly use equality constraints, following the results in [4] which show that the corresponding inequality constraints on final values are always active [refer to the discussion in Section III-C.2]. As the decision variable $u = u(t)$ one can consider either the temperature $T = T(t)$ or the supersaturation $S = S(t)$. An input profile $S = S(t)$ determines uniquely the profile $T = T(t)$, which is ultimately used as the control variable in practice. With T as the control input, U could be defined as $U = [T_{\min}, T_{\max}]$. For instance, the bounds on T can be determined by the capabilities of the thermostat used for regulation. On the other hand, the bounds on S, $U = [S_{\min}, S_{\max}]$, restrict the batch operation within the metastable region.

D. Related works

This work presents a systematic approach to the solution of the optimal control problem based on the minimum principle for a batch crystallization process with *size-dependent* growth kinetics. The main ideas are firmly based and extend the previous works of the authors in [5], [6] and [4]. In [5] an infinite dimensional ODE system for the PBE (1a-1c) is introduced, while [4] provides a near-optimal solution for a batch crystallization process with *size-independent* growth kinetics by making use of the minimum principle.

II. Infinite dimensional system

A. Coordinate transformation

Consider the population balance equation in (1a-1c) with (2). Introduce new independent coordinates (τ,λ) by

$$\tau = \phi(t),\;\; \lambda = \psi(\ell),\quad t \geq 0,\;\; \ell \geq 0 \qquad (8)$$

where the mappings ϕ and ψ are defined as the solutions of the initial value problems

$$\frac{{\rm d}\phi}{{\rm d}t} = G_0(t),\quad \frac{{\rm d}\psi}{{\rm d}\ell} = \frac{1}{\gamma(\ell)},\quad \phi(0) = 0,\;\; \psi(0) = 0. \qquad (9)$$

As $G_0(t) > 0$ and $\gamma(\ell) > 0$ are assumed to hold, the functions $\phi : [0,t_f] \to [0,\tau_f]$ and $\psi : [0,\ell_f] \to [0,\lambda_f]$ are strictly monotone and bijective. Hence, the inverse functions $t = \phi^{-1}(\tau)$ and $\ell = \psi^{-1}(\lambda)$ are uniquely defined. [*Note:* We will rather use the notations $t = t(\tau)$ and $\ell = \ell(\lambda)$ instead.] The size-independent factor $G_0(t)$ of the growth rate is *a priori* unknown since it depends on the process evolution. Therefore, $\tau = \phi(t)$ and $t = t(\tau)$ must be integrated for online. The size-dependent growth rate term $\gamma(\ell)$ is, however, typically given, implying that $\lambda = \psi(\ell)$ [and its inverse $\ell = \ell(\lambda)$] can be *a priori* computed using (9).

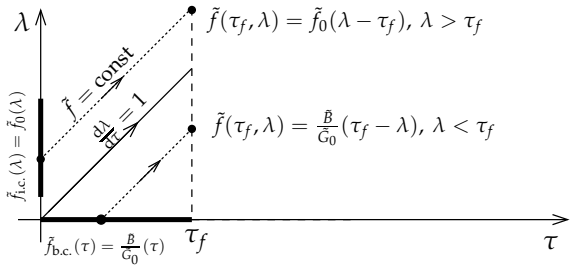

Fig. 1. Characteristic lines ($\mathrm{d}\lambda/\mathrm{d}\tau=1$) for the PBE (10a)-(10c).

The diffeomorphism maps (9) transform the original PBE (1a-1c) into a simple transport equation

$$\frac{\partial\tilde{f}}{\partial\tau}+\frac{\partial\tilde{f}}{\partial\lambda}=0,\ \lambda>0,\ \tau>0 \tag{10a}$$

$$\tilde{f}(\tau,0)=\frac{\tilde{B}}{\tilde{G}_0}(\tau),\ \tau\geq 0 \tag{10b}$$

$$\tilde{f}(0,\lambda)=\tilde{f}_0(\lambda),\ \lambda\geq 0 \tag{10c}$$

where the following settings hold

$$\tilde{f}(\tau,\lambda):=\gamma(\ell(\lambda))\cdot f(t(\tau),\ell(\lambda)) \tag{11a}$$

$$\tilde{B}(\tau):=B(t(\tau)) \tag{11b}$$

$$\tilde{G}_0(\tau):=G_0(t(\tau)) \tag{11c}$$

$$\tilde{f}_0(\lambda):=\gamma(\ell(\lambda))\cdot f_0(\ell(\lambda)). \tag{11d}$$

Equations (9) infer that the curves $\mathrm{d}\ell/\mathrm{d}t=\gamma(\ell)G_0(t):=G(t,\ell)$ map to $\mathrm{d}\lambda/\mathrm{d}\tau=1$ in the (τ,λ)-domain. It is the solution of the both latter equations, that is, $\int_0^\ell \mathrm{d}\xi/\gamma(\xi)=\int_0^t G_0(\eta)\mathrm{d}\eta$ in the (t,ℓ)-domain, and $\lambda=\tau$ in the (τ,λ)-domain, which defines the boundary in the underyling domain which separates the two functions f_{s} and f_{n}, see Section I-C. For any other initial conditions, $(t=0,\ell>0)$ in the (t,ℓ)-domain, and $(\tau>0,\lambda=0)$ in the (τ,λ)-domain, the solutions represent the *projected characteristic curves*. The *characteristic curves* for the PDE (10a), in particular, are directly given by the initial data which are propagated along the straight lines with unity slope, see Fig 1. The evolution of the density function in (10a) is then explicitly expressed in terms of the initial (*i.e.* seed) and boundary condition (*i.e.* nucleation) density functions

$$\tilde{f}(\tau,\lambda)=\begin{cases}\tilde{f}(\tau-\lambda,0)=\ \tilde{B}/\tilde{G}_0(\tau-\lambda),\ \lambda<\tau\\ \tilde{f}(0,\lambda-\tau)=\ \tilde{f}_0(\lambda-\tau),\qquad \lambda>\tau.\end{cases} \tag{12}$$

As a consequence, the integration of the PBE (10a-10c) reduces to the computation of the temporal evolution of the boundary density function $\tilde{B}/\tilde{G}_0(\tau)$. Therefore, next, a generalization of the method of moments will be used.

B. Convolution method of moments

Notice that, by definition, $\tilde{f}\mathrm{d}\lambda=f\mathrm{d}\ell$, implying $\int_0^\infty\tilde{f}(\tau,\lambda)\mathrm{d}\lambda=\int_0^\infty f(t,\ell)\mathrm{d}\ell$, which means that the 0^{th} moment of the density function f, μ_0, is an invariant of the coordinate transformation (8)-(9). Differentiation of the left hand-side term *w.r.t.* τ, after substitution of (10a) and integration by parts, reveals the ODE: $\dot{\mu}_0=\frac{\tilde{B}}{\tilde{G}_0}(\tau)$ [*Note:* The dot operator hereafter refers to $\partial/\partial\tau$]. Application of the same procedure for the moments $\mu_i(\tau)=\int_0^\infty\ell^i(\lambda)\tilde{f}(\tau,\lambda)\mathrm{d}\lambda$, $i=1,2,\ldots$, results with the following system of integro-differential equations

$$\dot{\mu}_0=\frac{\tilde{B}}{\tilde{G}_0}(\tau),\ \dot{\mu}_i=i\tilde{\mu}_{i-1}(\tau),\ i=1,2,\ldots \tag{13a}$$

where we are forced to introduce the moments of the scaled density function $\gamma(\ell)f(t,\ell)$

$$\tilde{\mu}_i(\tau):=\int_0^\infty\ell^i(\lambda)\tilde{\gamma}(\lambda)\tilde{f}\,(\tau,\lambda)\,\mathrm{d}\lambda,\ i=1,2,\ldots, \tag{14}$$

with $\tilde{\gamma}(\lambda):=\gamma(\psi^{-1}(\lambda))$. A structural reduction and a better insight into the process dynamics described by (13a) is gained if, again, the moments μ_i and $\tilde{\mu}_i$ are decomposed into the moments arising from the nucleation and seed population: $\mu_i=\mu_{i,\mathrm{n}}+\mu_{i,\mathrm{s}}$, and $\tilde{\mu}_i=\tilde{\mu}_{i,\mathrm{n}}+\tilde{\mu}_{i,\mathrm{s}}$, $i=0,1,2,\ldots$, with

$$\mu_{i,\mathrm{n}}(\tau):=\int_0^\tau\ell^i(\lambda)\frac{\tilde{B}}{\tilde{G}_0}(\tau-\lambda)\mathrm{d}\lambda, \tag{15a}$$

$$\tilde{\mu}_{i,\mathrm{n}}(\tau):=\int_0^\tau\ell^i(\lambda)\tilde{\gamma}(\lambda)\frac{\tilde{B}}{\tilde{G}_0}(\tau-\lambda)\mathrm{d}\lambda, \tag{15b}$$

$$\mu_{i,\mathrm{s}}(\tau):=\int_0^\infty\ell^i(\lambda+\tau)\tilde{f}_0(\lambda)\mathrm{d}\lambda, \tag{15c}$$

$$\tilde{\mu}_{i,\mathrm{s}}(\tau):=\int_0^\infty\ell^i(\lambda+\tau)\tilde{\gamma}(\lambda+\tau)\tilde{f}_0(\lambda)\mathrm{d}\lambda, \tag{15d}$$

where, additionally, the transport equations (12) have been substituted. It is hereof clear that the partial moments, $\mu_{i,\mathrm{s}}$ and $\tilde{\mu}_{i,\mathrm{s}}$, arising from the initial density function are driven by the "time" τ only, and, thus, can be integrated *a priori*, independently on the process evolution.

From (4) and (5) it is clear that the driving term $\tilde{B}/\tilde{G}_0$ in (15b) and (15b) is coupled to the 3^{rd} physical moment $\mu_3=\mu_{3,\mathrm{s}}+\mu_{3,\mathrm{n}}$, in that [with a slight abuse of notation]

$$\frac{\tilde{B}}{\tilde{G}_0}=\frac{\tilde{B}}{\tilde{G}_0}\left(u(\tau),\mu_3(\tau)\right), \tag{16}$$

where $u=u(\tau)$ may refer to the temperature $T=T(\tau)$ or the supersaturation $S=S(\tau)$ as the input variable. Moreover, the form of the net dynamics (13a) is inherited by the moments $\mu_{i,\mathrm{n}}$ and $\tilde{\mu}_{i,\mathrm{n}}$, leading to a closed moment model, involving an integro-differential equation

$$\dot{\mu}_{0,n}=\frac{\tilde{B}}{\tilde{G}_0}\left(u(\tau),\mu_{3,\mathrm{n}}(\tau)+\mu_{3,\mathrm{s}}(\tau)\right), \tag{17a}$$

$$\dot{\mu}_{3,n}=3\tilde{\mu}_{2,n}(\tau), \tag{17b}$$

where $\mu_{3,\mathrm{n}}(0)=0$, and $\tilde{\mu}_{2,\mathrm{n}}=\tilde{\mu}_{2,\mathrm{n}}(\tau)$ and $\tilde{\mu}_{3,\mathrm{s}}=\tilde{\mu}_{3,\mathrm{s}}(\tau)$ are given by the expressions (15b) and (15c), respectively. Note that both equations are coupled by the terms $\tilde{B}/\tilde{G}_0$ and $\mu_{3,\mathrm{n}}$, while the profile $\mu_{3,\mathrm{s}}(\tau)$ is fixed by

$$\mu_{3,\mathrm{s}}(\tau)=\int_0^\infty\ell^3(\lambda+\tau)\tilde{f}_0(\lambda)\mathrm{d}\lambda. \tag{17c}$$

Note that all solutions can be back-transformed to the "real" time t by including the equation

$$\dot{t}=\frac{1}{\tilde{G}_0}\left(u(\tau),\mu_{3,\mathrm{n}}(\tau)+\mu_{3,\mathrm{s}}(\tau)\right),\quad t(0)=0. \tag{17d}$$

C. Internal moment model

Introduce the *internal* or *eigenmoments* $\nu_i(\tau)$ of the density function $\tilde{f} = \tilde{f}(\tau, \lambda)$ in the (τ, λ)-domain as

$$\nu_i(\tau) = \int_0^\infty \lambda^i \tilde{f}(\tau, \lambda) \mathrm{d}\lambda, \quad i = 0, 1, 2, \ldots. \tag{18}$$

Then, it can be easily verified that the latter form a closed ODE structure in the $\tau-$domain, which we will be referring to as the *internal model*, given by

$$\dot{\nu}_0 = \frac{\tilde{B}}{\tilde{G}_0}(\tau), \quad \dot{\nu}_i = i\nu_{i-1}(\tau), \quad i = 1, 2, \ldots \tag{19}$$

This model is again inherited by the nucleation moments $\nu_{i,\mathrm{n}}$

$$\dot{\nu}_{0,\mathrm{n}} = \frac{\tilde{B}}{\tilde{G}_0}(\tau), \quad \dot{\nu}_{i,\mathrm{n}} = i\nu_{i-1,\mathrm{n}}(\tau), \ i = 1, 2, \ldots \tag{20}$$

and the seed moments $\nu_{i,\mathrm{s}}$, too

$$\dot{\nu}_{0,\mathrm{s}} = 0, \quad \dot{\nu}_{i,\mathrm{s}} = i\nu_{i-1,\mathrm{s}}(\tau), \ i = 1, 2, \ldots \tag{21}$$

where we use the decomposition $\nu_i = \nu_{i,\mathrm{n}} + \nu_{i,\mathrm{s}}$ with

$$\nu_{i,\mathrm{n}}(\tau) = \int_0^\tau \lambda^i \frac{\tilde{B}}{\tilde{G}_0}(\tau - \lambda) \mathrm{d}\lambda, \tag{22}$$

$$\nu_{i,\mathrm{s}}(\tau) = \int_0^\infty (\lambda + \tau)^i \tilde{f}_0(\lambda) \mathrm{d}\lambda. \tag{23}$$

From (21) it is easy to show that the evolution of the moments $\nu_{i,\mathrm{s}} = \nu_{i,\mathrm{s}}(\tau)$ can be simply expressed by an i^{th} order polynomial in τ

$$\nu_{i,\mathrm{s}}(\tau) = \sum\nolimits_{k=0}^{i} \binom{i}{k} \nu_{k,\mathrm{s}}(0)\, \tau^{i-k}, \tag{24}$$

where $\nu_{k,\mathrm{s}}(0)$ is the initial value of the moment $\nu_{k,\mathrm{s}}$. The eigenmoments $\nu_i = \nu_i(\tau)$ can not be associated a particular physical interpretation. However, as we now infer, they can be conveninetly used for a series approximation of the physical moments $\mu_i(\tau) = \mu_{i,\mathrm{n}}(\tau) + \mu_{i,\mathrm{s}}(\tau)$ from (15a) and (15c). Therefore, consider the expansion of $\ell^i(\lambda)$ in the power series at $\lambda = 0$

$$\ell^i(\lambda) = \sum\nolimits_{k=i}^{\infty} b_{ki} \lambda^k, \tag{25}$$

with coefficients b_{ki} being referred to as Bell coefficients, and defined by

$$b_{ki} = \frac{i!}{k!} B_{ki}\left(\gamma(0), D\gamma(0), \ldots, D^{k-i}\gamma(0)\right). \tag{26}$$

Here B_{ki} stands for the multivariate Bell polynomial (see [7]) in terms of the variables set by the operator $D := \gamma \frac{\mathrm{d}}{\mathrm{d}\ell}$ with $D^0 := 1$ and $D^j := D \cdot D^{j-1}$, for $j = 1, 2, \ldots$, where $D^j\gamma(0) := D^j\gamma(\ell)\big|_{\ell=0}$, $j = 0, 1, \ldots, k-i$.

Substituting (25) in (15a) reveals the required expansion of the moments $\mu_{i,\mathrm{n}}$ in terms of the eigenmoments $\nu_{k,\mathrm{n}}$

$$\mu_{0,\mathrm{n}}(\tau) = \nu_{0,\mathrm{n}}(\tau), \tag{27}$$

$$\mu_{i,\mathrm{n}}(\tau) = \sum\nolimits_{k=i}^{\infty} b_{ki} \nu_{k,\mathrm{n}}(\tau), \quad i = 1, 2, \ldots. \tag{28}$$

Using the Taylor polynomial representation, $\ell^i(\lambda) = \sum_{k=i}^{p} b_{ki}\lambda^k + R_p(\lambda)$. Then, there exists a positive constant M_p such that the remainder term is bounded, *i.e.* $|R_p(\lambda)| \leq M_p\tau^{p+1}/(p+1)!$ for $0 < \lambda < \tau$. Therefore,

$$\mu_{i,\mathrm{n}}(\tau) = \sum\nolimits_{k=i}^{p} b_{ki}\nu_{k,\mathrm{n}}(\tau) + O_p(\tau), \tag{29}$$

where $|O_p(\tau)| < \mu_{0,\mathrm{n}} M_p \tau^{p+1}/(p+1)!$, and $O_p(\tau) \to 0$ as $p \to \infty$. Hence, the moment $\mu_{i,\mathrm{n}}$ can be approximated at any level of accuracy by the finite sum in (29).

By applying the same derivation lines an analogous expansion to (29) can be derived for the moments $\mu_{i,\mathrm{s}}$ in terms of the eigenmoments $\nu_{i,\mathrm{s}}$. Indeed, using (24)

$$\mu_{ip,\mathrm{s}}(\tau) = \sum\nolimits_{k=i}^{p} a_{ki}\, \tau^k, \tag{30}$$

where we introduce the parameters

$$a_{ki} = \sum\nolimits_{j=\max(k,i)}^{p} b_{ji} \binom{j}{k} \nu_{j-k,\mathrm{s}}(0), \ k = 0, 1, \ldots, p. \tag{31}$$

This leads us to an ODE system, which we refer to as the *internal model* given by

$$\dot{\nu}_{0,\mathrm{n}} = \tfrac{\tilde{B}}{\tilde{G}_0}(u(\tau), \mu_{3p}(\tau)) \tag{32a}$$

$$\dot{\nu}_{1,\mathrm{n}} = \nu_{0,\mathrm{n}}(\tau) \tag{32b}$$

$$\ldots$$

$$\dot{\nu}_{p,\mathrm{n}} = p\nu_{p-1,\mathrm{n}}(\tau) \tag{32c}$$

where $\mu_{3p} = \mu_{3p,\mathrm{n}} + \mu_{3p,\mathrm{s}}$, that is

$$\mu_{3p}(\tau) = \sum\nolimits_{k=3}^{p} b_{k3}\nu_{k,\mathrm{n}}(\tau) + \sum\nolimits_{k=0}^{p} a_{k3}\, \tau^k. \tag{32d}$$

For $p < \infty$, the internal model provides an *approximate ODE system* that can be used for the computation of the evolution of the moment $\mu_3 = \mu_3(\tau)$, and of the density function $\tilde{f} = \tilde{f}(\tau, \lambda)$ using (16) and (12). For $p = \infty$, the solutions converge to the exact ones provided by the convolution method of moments using (17a)-(17c).

III. Optimal control

A. Optimization problem

Referring to the introductory notes on the problem formulation in Section I-C, the optimization problem is restated here in the τ-domain, as follows

$$\underset{u(\tau)\in U,\, \tau\in[0,\tau_f]}{\text{minimize}}\ \mu_{3,\mathrm{n}}(\tau_f) \text{subject to} \begin{array}{rcl} \tau_f & = & \tau_{f,c} \\ t(\tau_f) & = & t_{f,c}. \end{array} \tag{33}$$

Note that the first equality constraint $\mu_{3,\mathrm{s}}(\tau_f) = \mu_{3f,\mathrm{sc}}$ in (6) is here substituted by $\tau_f = \tau_{f,c}$. With regard to (17c), this is an equivalent constraint. Indeed, (17c) infers that given $\mu_{3,\mathrm{s}}(\tau_f) = \mu_{3f,\mathrm{sc}}$, the final time instant τ_f is fixed at some value $\tau_{f,c}$, which can be obtained by solving numerically $\mu_{3,\mathrm{s}}(\tau_f) = \mu_{3f,\mathrm{sc}}$ in (17c) for τ_f.

We will find it convenient to select the inverse of the growth rate as the input variable, namely, we use $u(\tau) \triangleq 1/\tilde{G}_0(\tau)$, and set fixed bounds on this variable, that is

$$U = \left[\left(\tfrac{1}{G_0}\right)_{\min}, \left(\tfrac{1}{G_0}\right)_{\max}\right]. \tag{34}$$

Moreover, we will allow $\left(\frac{1}{G_0}\right)_{\max}$ to be chosen arbitrarily large. Note that the limitation $\left(\frac{1}{G_0}\right)_{\min}$ restricts the operation

within the metastable region. Due to the second equation in (4), the selection of $1/\tilde{G}_0$ as the input is an equivalent reformulation of the supersaturation as input. Of course, for a given trajectory $u = u(\tau)$, the corresponding optimal profile of the cooling temperature $T = T(\tau)$ will be uniquely determined by the evolution of the system dynamics, as well. Moreover, it is easy to check that with this definition for u

$$\frac{\tilde{B}}{\tilde{G}_0}(u, \mu_3) = k_b\, k_g^{-\frac{b}{g}}\, u^{-\frac{b-g}{g}}\, \mu_3. \tag{35}$$

B. Idealized internal moment model

For convenience, introduce the extended system state $\mathbf{x} = [x_1, x_2, \ldots, x_{p+2}]^T$, where

$$x_1 \hat{=} \nu_{p,\mathrm{n}},\ x_2 \hat{=} \nu_{p-1,\mathrm{n}},\ \ldots,\ x_{p+1} \hat{=} \nu_{0,\mathrm{n}},\ x_{p+2} \hat{=} t.$$

The approximate internal model (32a-32c) including the time equation (17d) reads

$$\dot{x}_1 = p x_2 \tag{36a}$$
$$\dot{x}_2 = (p-1) x_3 \tag{36b}$$
$$\cdots$$
$$\dot{x}_p = x_{p+1} \tag{36c}$$
$$\dot{x}_{p+1} = \tfrac{\tilde{B}}{\tilde{G}_0}(u(\tau), \mu_{3p,\mathrm{s}}(\tau) + \mu_{3p,\mathrm{n}}(\tau)) \tag{36d}$$
$$\dot{x}_{p+2} = u(\tau), \tag{36e}$$

with $u(\tau) \hat{=} 1/\tilde{G}_0(\tau)$ as the control input. Now, we propose a model simplification that will substantially alleviate the solution to our optimal control problem. We will, namely, negelect the feedback of $\mu_{3p,\mathrm{n}}(\tau) = \sum_{k=3}^{p} b_{k3} x_{p-k+1}(\tau)$, in the term $\tilde{B}/\tilde{G}_0$ in (36d), that is, replace the latter by

$$\dot{x}_{p+1} \approx \frac{\tilde{B}}{\tilde{G}_0}\left(u(\tau), \mu_{3p,\mathrm{s}}(\tau)\right), \tag{36f}$$

as well as its feedback in the mass-balance law (5), *i.e.*

$$m_{\mathrm{c}}(\tau) \approx m_0 - \rho k_v (\mu_{3p,\mathrm{s}}(\tau) - \mu_{3,0}). \tag{36g}$$

Effectively, the entire effect of $\mu_{3p,\mathrm{n}}$ into the crystallization kinetics (4)-(5) is neglected. This is intuitively justified by the fact that we expect to keep $\mu_{3p,\mathrm{n}}(\tau) \ll \mu_{3p,\mathrm{s}}(\tau)$ for all $\tau \in [0, \tau_f]$, as the task of the optimization scheme is the very minimization of $\mu_{3p,f,\mathrm{n}} = \mu_{3p,\mathrm{n}}(\tau_f)$. In the sequel, we refer to this as the *idealization condition*, and to model (36a)-(36g) as the *idealized internal moment model*. On the other hand, the model (36a)-(36e), where the feedback of $\mu_{3p,\mathrm{n}}$ in the process kinetics is retained, will be referred to as the *real internal moment model*. Note that for $p = \infty$, the latter represents the *exact model* (17a)-(17d) given by the convolution method of moments.

Remark: By neglecting the feedback of $\mu_{3p,\mathrm{n}}(\tau)$ to the term $\tilde{B}/\tilde{G}_0$, (36a-36d) turns to a *linear time-invariant* system with a redefinition of the input as $u_1 = u^{1-b/g}\mu_{3p,\mathrm{s}}$. This is a useful fact, as the existing rich set of the control tools for linear systems can be applied here without further ado.

C. Optimal control solutions

Following the model reduction by the idealized internal model in the previous section, the optimal control problem (33) must be slightly reformulated as

$$\underset{u(\tau)\in U,\, \tau\in[0,\tau_f]}{\text{minimize}}\ \mu_{3p,\mathrm{n}}(\tau_f) \ \text{subject to}\ \begin{array}{rcl} \tau_f & = & \tau_{p,f,c} \\ t(\tau_f) & = & t_{f,c}. \end{array} \tag{37}$$

where the constraint constant $\tau_{p,f,c}$ is computed by solving $\mu_{3p,s}(\tau_f) = \mu_{3f,\mathrm{sc}}$ for τ_f using (30).

1) Minimum principle: Next, we consider the necessary conditions for an optimal trajectory. With reference to (29) our cost function is given by

$$\phi\left(\mathbf{x}(\tau_f), \tau_f\right) = \sum\nolimits_{k=3}^{p} b_{k3} x_{p-k+1}(\tau_f), \tag{38}$$

leading to the Hamiltonian $H(\mathbf{x}, u, \boldsymbol{\psi}, \tau) = \boldsymbol{\psi}^T \dot{\mathbf{x}}$

$$\begin{aligned} H(\mathbf{x}, u, \boldsymbol{\psi}, \tau) &= \\ &= p\psi_1 x_2 + (p-1)\psi_2 x_3 + \ldots + \psi_p x_{p+1} \\ &\quad + \psi_{p+1} \tfrac{\tilde{B}}{\tilde{G}_0}\left(u, \mu_{3p,\mathrm{s}}(\tau)\right) + \psi_{p+2} u, \end{aligned} \tag{39}$$

where $\boldsymbol{\psi}^T = [\psi_1, \ldots, \psi_{p+2}]$ includes the adjoint state of $\mathbf{x}$, defined by $\dot{\boldsymbol{\psi}} = -\partial H/\partial \mathbf{x}$, *i.e.*

$$\dot{\psi}_1 = 0, \tag{40a}$$
$$\dot{\psi}_2 = -p\psi_1, \dot{\psi}_3 = -(p-1)\psi_2, \ldots, \dot{\psi}_{p+1} = -\psi_p, \tag{40b}$$
$$\dot{\psi}_{p+2} = 0. \tag{40c}$$

The initial boundary conditions for the states are $\mathbf{x}(0) = \mathbf{0}$, while the final states $\mathbf{x}(\tau_f)$ are required to lie on the surface $m(\mathbf{x}(\tau)) := x_{p+2}(\tau) - t_{f,c} = 0$, and the final "time" τ_f is fixed. The boundary conditions for $\boldsymbol{\psi}^*(\tau_f)$ read, see [8]

$$\frac{\partial \phi}{\partial \mathbf{x}}(\mathbf{x}^*(\tau_f)) - \boldsymbol{\psi}^*(\tau_f) = C \frac{\partial m}{\partial \mathbf{x}}(\mathbf{x}^*(\tau_f)) \tag{41}$$

where $C \in \mathbb{R}$ is an unknown constant. Then the following terminal conditions for the adjoint states result

$$\psi_k(\tau_f) = b_{p-k+1,3},\ k = 1, 2, \ldots, p-2, \tag{42a}$$

and

$$\psi_{p-1}(\tau_f) = \psi_p(\tau_f) = \psi_{p+1}(\tau_f) = 0, \tag{42b}$$

since $x_{p+1} \hat{=} \nu_{0,\mathrm{n}}$, $x_p \hat{=} \nu_{1,\mathrm{n}}$ and $x_{p-1} \hat{=} \nu_{2,\mathrm{n}}$ are neither part of the cost function nor of the constraints. Using the latter conditions, the evolution of all adjoint states $\psi_k = \psi_k(\tau)$ for $k = 1, 2, \ldots, p+1$ from (40a-40b) can be readily computed in the analytic form

$$\psi_k(\tau) = \sum\nolimits_{j=1}^{k} b_{p-j+1,3} \binom{p-j+1}{k-j} (\tau_f - \tau)^{k-j}. \tag{43}$$

Hereby, one has to pay attention that for the parameters $b_{0,3}$, $b_{1,3}$ and $b_{2,3}$ which enter the expression (43) for the costates ψ_{p-1}, ψ_p, and ψ_{p+1}, the condition $b_{0,3} = b_{1,3} = b_{2,3} = 0$ applies. Moreover, using (25), it can be directly shown that the following useful fact holds

$$\lim_{p\to\infty} \psi_{p+1}(\tau) = \ell^3(\tau_f - \tau). \tag{44}$$

To summarize, the only unknown variable remains the costate ψ_{p+2}, which is constant [see (40c)], $\psi_{p+2}(\tau) = \text{const}$.

According to the minimum principle, the optimal control input $\breve{u}_p^*$ must satisfy

$$\begin{aligned}\breve{u}_p^* &= \underset{u\in U}{\operatorname{argmin}}\, H\left(\mathbf{x}, u, \boldsymbol{\psi}, \tau\right)\\ &= \underset{u\in U}{\operatorname{argmin}} \left(\psi_{p+1}\frac{\tilde{B}}{\tilde{G}_0}(u, \mu_{3p,\mathrm{s}}) + \psi_{p+2}u\right)\\ &= \underset{u\in U}{\operatorname{argmin}} \left(\psi_{p+1}k_b k_g^{-\frac{b}{g}} u^{-\frac{b-g}{g}}\mu_{3p,\mathrm{s}} + \psi_{p+2}u\right), \quad (45)\end{aligned}$$

where U is the compact set of the allowed input values (34). [*Note:* The accent '˘' in $\breve{u}_p^*$ is used to discriminate it from the optimal solution u_p^*, associated with the real internal moment model, see Section IV!] A candidate for the minimizing solution, which we denote by $\breve{u}_p^o$, is obtained by solving $\partial H/\partial u = 0$ for u

$$\breve{u}_p^o\left(\tau\right) = \frac{1}{k_g}\left(\frac{\psi_{p+1}\left(\tau\right)}{\psi_{p+2}}\frac{b-g}{g}k_b\mu_{3p,\mathrm{s}}\left(\tau\right)\right)^{\frac{g}{b}}. \quad (46)$$

2) Optimal solution, $p < \infty$: Consider the predominant case in practice with $b > g$. Due to $\psi_{p+1}(\tau) > 0$ for all $\tau \in [0, \tau_f)$ (refer to (44)), the first summand in (45) possesses a hyperbolic shape, taking the maximum value at $u_{\min} = (\frac{1}{\tilde{G}_0})_{\min}$, and the minimum at $u_{\max} = (\frac{1}{\tilde{G}_0})_{\max}$. The situation $\psi_{p+2} \leq 0$ would obviously lead to the conclusion $\breve{u}_p^* = u_{\max}$. However, a sufficiently large $u_{\max}$ could be always defined, such that $x_{p+2}(\tau_f) = t_f > t_{f,c}$, inferring that the time-constraint is violated. Hence, $\psi_{p+2} > 0$ must hold. [In addition, this confirms, that the equality constraint $t(\tau_f) = t_{f,c}$ must be active, as remarked in the introduction in Section I-C.] The term inside the parentheses in (46) is then positive, and the Hamiltonian function in (39) strictly convex. As time progresses the nonlinear term in (45) diminishes, and, eventually, at $\tau = \tau_f$ it becomes zero since according to (42b), $\psi_{p+1}(\tau_f) = 0$. Hence, a "time" instant $\tau_{\mathrm{c}} \in (0, \tau_f)$ must exist, such that $\breve{u}_p^o(\tau_{\mathrm{c}}) = u_{\min}$, and $\breve{u}_p^o\left(\tau\right) < u_{\min}$ for $\tau \in (\tau_{\mathrm{c}}, \tau_f]$, see Fig 2. In other words, the optimal solution $\breve{u}_p^*$ reads

$$\breve{u}_p^* = \begin{cases} \max(\breve{u}_p^o, u_{\min}), & 0 \leq \tau < \tau_{\mathrm{c}}\\ u_{\min}, & \tau_{\mathrm{c}} \leq \tau \leq \tau_f. \end{cases} \quad (47)$$

[*Note:* As indicated in Fig. 2 by dashed lines, and referring to (46), the behavior of the function $\breve{u}_p^o\left(\tau\right)$ can take different shapes for $\tau \in [0, \tau_{\mathrm{c}}]$, depending on the product $\psi_{p+1}(\tau)\mu_{3p,\mathrm{s}}(\tau)$, whereby the first term is strictly decreasing, and the second one strictly increasing in τ. Of course, for some τ in this interval, $\breve{u}_p^o\left(\tau\right) < u_{\min}$ may happen. Hence, we need the $\max$ operator in (47).]

3) Optimal solution for $p \to \infty$: Due to the approximation by the finite dimensional model (36a-36d), the obtained solution $\breve{u}_p^*$ is itself an approximation of the optimal solution $\breve{u}_\infty^*$, which refers to the infinite dimensional system with $p = \infty$. The latter follows directly from (47)

$$\breve{u}_\infty^* = \begin{cases} \max(\breve{u}_\infty^o, u_{\min}), & 0 \leq \tau < \tau_{\mathrm{c}}\\ u_{\min}, & \tau_{\mathrm{c}} \leq \tau \leq \tau_f. \end{cases} \quad (48)$$

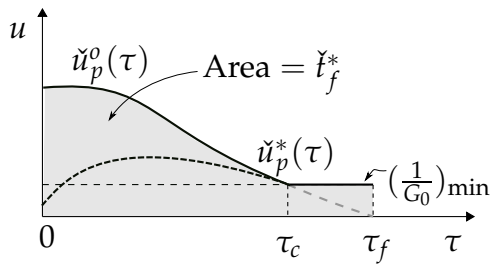

Fig. 2. The optimal solution profile.

where, $\breve{u}_\infty^o = \lim_{p\to\infty}\breve{u}_p^o$ with regard to (44), reads

$$\breve{u}_\infty^o\left(\tau\right) = \frac{1}{k_g}\left(\frac{k_b}{\psi_{p+2}}\frac{b-g}{g}\ell^3(\tau_f-\tau)\mu_{3,s}\left(\tau\right)\right)^{\frac{g}{b}}. \quad (49)$$

4) Convolution method: Consider the convolution integral (15a) used for the computation of $\mu_{3,\mathrm{n}} = \mu_{3,\mathrm{n}}\left(\tau\right)$. Introduce a modified convolution integral

$$\bar{\mu}_{3,\mathrm{n}}(\tau) = \int_0^\tau \ell^3(\tau_f-\lambda)\frac{\tilde{B}}{\tilde{G}_0}(\lambda)\mathrm{d}\lambda, \quad (50)$$

and, observe by comparing to (15a), that $\bar{\mu}_{3,\mathrm{n}}(\tau_f) = \mu_{3,\mathrm{n}}(\tau_f)$. Given the idealization condition, we can obviously dispense with the exact evolution of the variable $\mu_{3,\mathrm{n}}(\tau)$ for $\tau \in [0, \tau_f]$, and keep track of its final value only instead. Introduce now the states $x_1 \triangleq \bar{\mu}_{3,\mathrm{n}}$ and $x_2 \triangleq t$, and consider the ODE model

$$\dot{x}_1 = \ell^3(\tau_f-\tau)\frac{\tilde{B}}{\tilde{G}_0}\left(u(\tau), \mu_{3,\mathrm{s}}(\tau)\right), \quad \dot{x}_2 = u(\tau), \quad (51)$$

where we again use the idealization condition (36f). Referring to our original optimal control problem (33), the Hamiltonian reads

$$H = \psi_1\ell^3(\tau_f-\tau)k_b k_g^{-\frac{b}{g}}u^{-\frac{b-g}{g}}\mu_{3,\mathrm{s}}(\tau) + \psi_2 u, \quad (52)$$

with $\dot{\psi}_1 = -\partial H/\partial x_1$ and $\dot{\psi}_2 = -\partial H/\partial x_2$. This reveals the fact that both adjoint states are constant $\psi_1 = \text{const}$ and $\psi_2 = \text{const}$. From (41) it follows $\psi_1 = 1$, since $\phi = x_1(\tau_f)$. Then, the unconstrained minimizing solution, obtained by solving $\partial H/\partial u = 0$ for u, reads

$$\breve{u}^o\left(\tau\right) = \frac{1}{k_g}\left(\frac{k_b}{\psi_2}\frac{b-g}{g}\ell^3(\tau_f-\tau)\mu_{3,s}\left(\tau\right)\right)^{\frac{g}{b}}. \quad (53)$$

Hence, we derive exactly the same optimal solution as for $p = \infty$.

5) Uniqueness of the optimal solution: Since the profile of the product $\psi_{p+1}\left(\tau\right)\mu_{3p,\mathrm{s}}\left(\tau\right)$ in (46) is fixed in τ, ψ_{p+2} is the only "tuning" parameter influencing the process length

$$\breve{t}_f^* = \int_0^{\tau_f}\breve{u}_p^*(\tau)\ \mathrm{d}\tau \quad (54)$$

by scaling the unconstrained optimal solution $\breve{u}_p^o(\tau)$, as indicated in Fig. 2. From (46) it is clear that $\breve{u}_p^o(\tau)$ is a strictly decreasing function in ψ_{p+2}, and a value Ψ must exist, such that for $\psi_{p+2} > \Psi$, $\max(\breve{u}_p^o(\tau)) \leq u_{\min}$. This interval is, however, not of interest, as it is dropped by the condition $t_{f,c} > u_{\min}\tau_f$, which is mandatory, otherwise the optimal problem (33) would have been infeasible. As

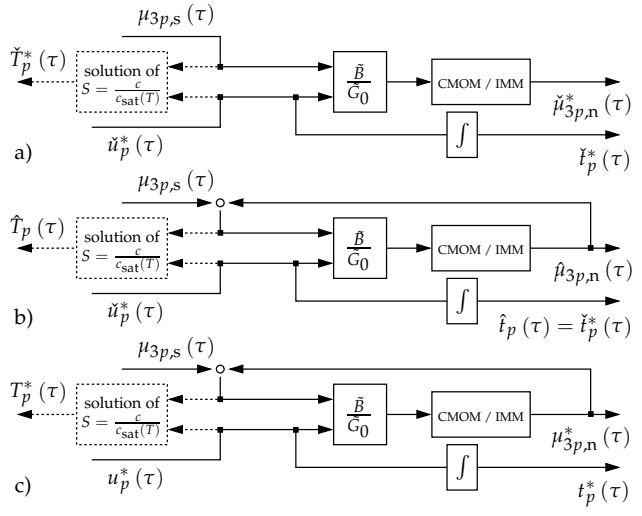

Fig. 3. Error analysis due to the idealization condition: a) Idealized model, controlled by $\check{u}_p^*$; b) Real model excited by (the same input) $\check{u}^*$; c) Real model under optimal control $\check{u}_p^*$. [Abbr., CMOM: Convolution method of moments (Section II-B), and IMM: Internal moment model (Section II-C).]

a consequence, in the interval of interest, $0 < \psi_{p+2} < \Psi$, the process duration is itself strictly decreasing in ψ_{p+2}, as well. The value at $\check{\psi}_{p+2}^*$ has to be selected such that the time constraint in (33) and (37) is satisfied. Such a solution is then unique, and as a consequence, the optimal solution constructed by (47) and (48) is itself *unique*.

IV. Sub-optimality bounds

The solution of the optimal control problem yields not only $\check{u}_p^*(\tau)$, where $p < \infty$ or $p = \infty$, but also the state trajectory $\check{\mathbf{x}}^*(\tau)$ and, amongst others, the supersaturation $\check{S}_p^*(\tau)$. For realization of the profile $\check{u}_p^*(\tau)$ by manipulating $\check{T}_p^*(t)$ in the "real" time t, two further steps need to be accomplished:

(i) Compute $\check{T}_p^*(\tau)$ by solving the algebraic equation $c_{\rm sat}(\check{T}_p^*(\tau)) = \check{c}_p^*(\tau)/\check{S}_p^*(\tau)$ for $\check{T}_p^*(\tau)$ in $\tau \in [0, \tau_f]$, where $\check{c}_p^*(\tau) = \check{m}_{{\rm c},p}^*(\tau)/(m_{\rm W} + \check{m}_{{\rm c},p}^*(\tau))$, and $\check{m}_{{\rm c},p}^*(\tau)$ is computed using the simplified mass balance equation (36g), (see Section I-B);

(ii) Convert $\check{T}_p^*(\tau)$ to $\check{T}_p^*(t)$ using the trajectory $\check{t}_p^*(\tau) = \check{x}_{p+2}^*(\tau)$.

The computed temperature profile $\check{T}_p^*(t)$ [again, p may be finite or ∞], which is optimal for the idealized internal model (36a)-(36f) is not optimal *w.r.t.* a model corresponding to a different value of p, or a model which retains the feedback of $\mu_{3p,{\rm n}}(t)$ in the crystallization kinetics (4)-(5) (the *real internal moment model*). The optimality of the profile $\check{T}_p^*(t)$ is then lost for two reasons: either the cost function is not minimal, while the constraints are held when the input profile $\check{T}_p^*(t)$, $t \in [0, t_f]$ is applied, or, more likely, some or all constraints are violated. In the latter case, comparing the costs does not make sense.

In this section, we discuss the errors in the solution of the optimal control problem resulting from the use of the idealization conditions (36f)-(36g). Thereby, at our focus are the idealized and the real internal moment models with a fixed order p, where $p \leq \infty$. Ultimately, we will construct a feasible sub-optimal temperature profile in the "real" time, $\hat{T}(t)$, which guarantees the constraints, and provides an upper bound for the minimal possible cost.

Therefore, consider Fig. 3, with three scenarios of interest depicted schematically. All contain a dotted block for the computation of the respective temperature profiles according to the method explained under the item *(i)*. Note that, thereby, for the schemes in Figs. 3b) and 3c), in *(i)*, the mass balance law (5) in the τ-domain with $\mu_{3p}(\tau) = \mu_{3p,{\rm s}}(\tau) + \mu_{3p,{\rm n}}(\tau)$ is to be used instead of (36g). Fig. 3a) refers to the idealized internal moment model (36a)-(36f): notice that the feedback from $\check{\mu}_{3p,{\rm n}}^*$ is missing, while in the real moment model in Figs. 3b) and 3c) the feedback is present. The scenarios in Figs. 3b) and 3c) differ, in that the scheme in Fig. 3b) is driven by the idealized optimal control $\check{u}_p^*$, while the one in Fig. 3c) is controlled by the correct [yet unknown!] optimal solution u_p^*.

From (35) it follows that for $\mu_{3p,{\rm n}} \geq 0$ and any u

$$\tfrac{\tilde{B}}{\tilde{G}_0}(u_p^*, \mu_{3p,{\rm s}} + \mu_{3p,{\rm n}}) \geq \tfrac{\tilde{B}}{\tilde{G}_0}(u_p^*, \mu_{3p,{\rm s}}).$$

Note also that $(\tilde{B}/\tilde{G}_0)'(\tau) \geq (\tilde{B}/\tilde{G}_0)''(\tau)$ for $0 \leq \tau \leq \tau_f$, implies $\mu'_{3p,{\rm n}}(\tau) \geq \mu''_{3p,{\rm n}}(\tau)$ [since (36a)-(36d) is a chain of integrators], where $\mu'_{3p,{\rm n}}(\tau)$ and $\mu''_{3p,{\rm n}}(\tau)$ represent the responses corresponding to the inputs $(\tilde{B}/\tilde{G}_0)'(\tau)$ and $(\tilde{B}/\tilde{G}_0)''(\tau)$, respectively. As a consequence, for any fixed input $u(\tau)$ applied to both schemes in Figs. 3a) and 3c), the resulting $\mu_{3p,{\rm n}}(\tau)$ in Fig. 3c) will be larger than that in Fig. 3a) for all $0 \leq \tau \leq \tau_f$. In particular, the cost $\mu_{3p,{\rm n}}(\tau_f)$ in Fig. 3c) is not lower than that in Fig. 3a). Therefore, if $u(\tau) = u_p^*(\tau)$ would be applied to the idealized model in Fig. 3a), the resulting cost $\bar{\mu}_{3p,{\rm n}}(\tau_f)$ would be lower or equal to $\mu_{3p,{\rm n}}^*(\tau_f)$, while the final time $\bar{t}_f$ would be equal to t_f^*, indicating that the time constraint in the optimal problem (37) is held. Moreover, as $\check{\mu}_{3p,{\rm n}}^*(\tau_f) \leq \bar{\mu}_{3p,{\rm n}}(\tau_f)$, we conclude $\check{\mu}_{3p,{\rm n}}^*(\tau_f) \leq \mu_{3,{\rm n}}^*(\tau_f)$.

Next, we apply the idealized optimal control $\check{u}_p^*(\tau)$ as the input to the real model in Fig. 3b). [*Note:* The resulting system variables in this scenario are denoted by the hat '$\hat{}$' attribute, for instance, $\hat{T}_p(\tau)$, $\hat{t}_p(\tau)$, $\hat{\mu}_{3p,{\rm n}}(\tau)$.] Again, the time constraint is held, that is, $\hat{t}_{p,f} = \check{t}_{p,f}^* = t_{f,c}$. However, as $\check{u}_p^*(\tau)$ is not the optimal solution for the underlying model, $\mu_{3p,{\rm n}}^*(\tau_f) \leq \hat{\mu}_{3p,{\rm n}}(\tau_f)$. Hence, we reach to the conclusion

$$\check{\mu}_{3p,{\rm n}}^*(\tau_f) \leq \mu_{3p,{\rm n}}^*(\tau_f) \leq \hat{\mu}_{3p,{\rm n}}(\tau_f). \qquad (55)$$

Finally, for realization of $\check{u}_p^*(\tau)$ in Fig. 3b), the resulting profile $\hat{T}_p(\tau)$ has to be transformed to $\hat{T}_p(t)$ in the "real" time by making use of $\hat{t}_p(\tau)$, which, as indicated in the figure, coincides with the $\check{t}_p^*(\tau)$ in the item *(ii)*.

To summarize, we suggest the input profile $\hat{T}_p = \hat{T}_p(t)$, $t \in [0, t_{f,c}]$, as a convenient sub-optimal solution to the optimal control problem (37) for the real internal moment model (36a)-(36e) [the feedback of $\mu_{3p,{\rm n}}$ in the process kinetics is present!]. Note that this is a feasible solution, in that it guarantees both constraints, $t_f = t_{f,c}$, and $\tau_f = \tau_{f,c}$ (*i.e.* , $\mu_{3,s}(t_f) = \mu_{3f,{\rm sc}}$). Additionally, according to (55),

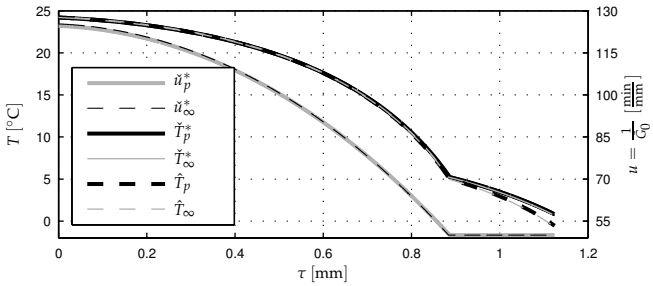

Fig. 4. Control in τ-domain.

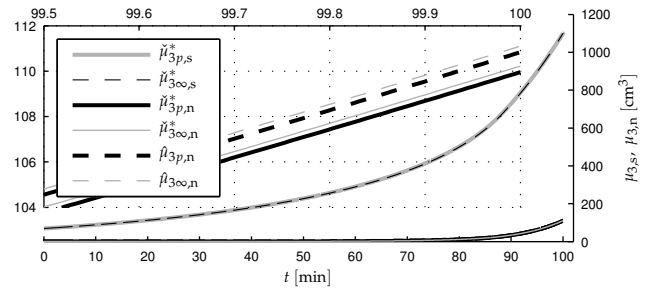

Fig. 5. Evolution of the third moments in t-domain.

the upper and lower bounds for the minimal possible cost $\mu_{3p,\text{n}}^*(\tau_f)$ are available, too. In particular, for the exact model given by (17a)-(17d), or the infinite dimensional real internal moment model, use $\hat{T}_\infty$ as the near-optimal solution.

V. Numerical example

Figs. 4 and 6 show the optimal control solutions for the idealized internal moment model for $p = 8$ ($\check{u}_p^*$, $\check{T}_p^*$), and $p = \infty$ ($\check{u}_\infty^*$, $\check{T}_\infty^*$), as well as the corresponding sub-optimal ones for the real internal moment model ($\hat{T}_p$ and $\hat{T}_\infty$), computed using our approach, in the τ- and t-domain, respectively. The computed optimal trajectories exhibit the common steep drop in the temperature at the end, corresponding to a [not shown] surge in the supersaturation profile. In addition, the constant tails, $\check{u}_p^* = (\frac{1}{G_0})_{\min}$ and $\check{u}_\infty^* = (\frac{1}{G_0})_{\min}$, at the process end, are clearly visible, as predicted in Section III-C, refer to Fig. 2.

In Fig. 5 we plot the resulting evolution of the third moments: $\mu_{3,\text{n}}$ and $\mu_{3,\text{s}}$. A large zooming shows a tight match of all cost function values $\check{\mu}_{3p,\text{n}}^*$, $\check{\mu}_{3\infty,\text{n}}^*$, $\hat{\mu}_{3p,\text{n}}$ and $\hat{\mu}_{3\infty,\text{n}}$ at $t = t_{f,c} = 100$[min], which confirms the near-optimality of our sub-optimal solutions $\hat{T}_p(t)$ and $\hat{T}_\infty(t)$. Towards the end, the effect of $\mu_{3p,\text{n}}$ and $\mu_{3\infty,\text{n}}$ via the mass-balance law (5) in the process kinetics, becomes substantial, leading to a noticable correction in the profiles of $\hat{T}_p$ and $\hat{T}_\infty$, see Figs. 4 and 6.

Note that the parameters and initial conditions for the case study are adopted from [6], and are listed in Table I.

Process parameters:
$k_b = 3.4177 \cdot 10^7 \frac{1}{\text{m}^3 s}$; $b = 2.3463$; $k_g = 1.3718 \cdot 10^{-5} \frac{m}{s}$; $g = 0.7253$
$a_0 = 0.0257$; $a_1 = 1.2 \cdot 10^{-3} \frac{1}{^\circ\text{C}}$; $a_2 = 3.442 \cdot 10^{-5} \frac{1}{^\circ\text{C}^2}$; $\rho = 1250 \frac{\text{kg}}{\text{m}^3}$; $k_v = 0.0288$
Linear C-R model: $\gamma(\ell) = 1 + \alpha\ell$; $\alpha = 400 \frac{1}{\text{m}}$;
Initial conditions:
$f_0(\ell) = \frac{1}{\eta_0} \cdot N(\ell)$; $N(\ell) = \mathcal{N}(\ell; \bar{\mu}_1, \sigma_1^2) + \mathcal{N}(\ell; \bar{\mu}_2, \sigma_2^2))$; $\mathcal{N} \rightarrow$ normal distribution
$\bar{\mu}_1 = 8 \cdot 10^{-4}$; $\sigma_1 = 1.7 \cdot 10^{-4}$; $\bar{\mu}_2 = 16 \cdot 10^{-4}$; $\sigma_2 = 2.5 \cdot 10^{-4}$; $\eta_0 = \frac{m_s}{\rho k_v \int_0^\infty \ell^3 N(\ell) \text{d}\ell}$
$m_s = 2.5 \cdot 10^{-3}$kg; $m_\text{w} = 0.8017$ kg; $m_0 = 0.09915$ kg

TABLE I

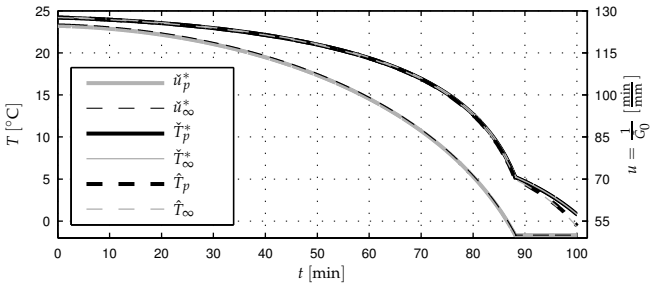

Fig. 6. Control in t-domain.

Moreover, $t_{f,c} = 100$ [min], $(\frac{1}{G_0})_{\min} = 5$ [min/mm], and $\mu_{3f,sc} = 1100$ [cm^3] are used. As a case study, the linear model with $\gamma(\ell) = 1 + \alpha\ell$ has been utilized.

VI. Conclusion

We have presented a systematic method for the solution to the optimal control problem for a batch crystallizer with size-dependent growth kinetics. The method is based on a transformation of the independent time and size variables of the underlying population balance equation that eventually leads to a closed infinite dimensional moment model and its finite order approximation. The goal of the posed optimization problem consists in minimizing the nucleation mass, while producing a specified amount of the mass of grown crystal seeds, within some given time scope. The optimal control problem is solved using the minimum principle for both, a finite and an infinite dimensional idealized model, where the entire feedback of the nucleation mass into the process kinetics is neglected. A sub-optimal cooling temperature profile which guarantees the constraints is suggested as a simple and feasible near-optimal solution for the optimization problem involving the exact model. An upper and a lower bound for the cost are provided, as well. It has been argued and illustrated by a numerical example, that the error is sufficiently small when the goal consists in suppressing the nucleation.

References

[1] A. S. Myerson, *Handbook of Industrial Crystallization*. Boston [u.a.] Butterworth-Heinemann, 2002.

[2] A. D. Randolph and M. A. Larson, *Theory of Particulate Processes*. Academic Press, Inc, 1988.

[3] R. Gunawan, I. Fusman, and R. D. Braatz, "High resolution algorithms for multidimensional population balance equations," *AIChE Journal*, vol. 50, no. 11, pp. 2738–2749, 2004.

[4] S. Hofmann and J. Raisch, "Application of optimal control theory to a batch crystallizer using orbital flatness," *16th Nordic Process Control Workshop, Lund, Sweden, 25-27th of August 2010; Nordic Working Group on Process Control*, 2010.

[5] N. Bajcinca, S. Qamar, and D. Flockerzi, "Methods for integration and dynamic inversion of population balance equations with size-dependent growth rate," *4th International Conference on Population Balance Modelling, Berlin*, 2010.

[6] N. Bajcinca, "Forward and inverse integration of population balance equations with size-dependent growth rate," *DYCOPS 2010, 9th International Symposium on Dynamics and Control of Process Systems, 2010, Leuven Belgium*, 2010.

[7] E. T. Bell, "Partition polynomials," *Ann. of Math*, vol. (2)29, no. 1-4, pp. 38–46, 1927.

[8] D. E. Kirk, *Optimal Control Theory: An Introduction*. Dover Publications, 2004.